A circuit approach for the electromagnetic analysis of inhomogeneous cylindrical structures

Article *in* Progress In Electromagnetics Research B · May 2011

DOI: 10.2528/PIERB11040105

1 author:

Jose A Brandao Faria
University of Lisbon
153 PUBLICATIONS **1,196** CITATIONS

Progress In Electromagnetics Research B, Vol. 30, 223–238, 2011

A CIRCUIT APPROACH FOR THE ELECTROMAGNETIC ANALYSIS OF INHOMOGENEOUS CYLINDRICAL STRUCTURES

J. A. Brandão Faria

Instituto de Telecomunicações, Instituto Superior Técnico
Technical University of Lisbon
Av. Rovisco Pais, 1049-001 Lisboa, Portugal

Abstract—An equivalent circuit, made of the chain connection of a number of T-type two-port networks, is proposed for the very accurate representation of the frequency-domain behavior of radially inhomogeneous solitary cylindrical structures, the individual two-port networks being made of frequency-independent R, L and C lumped elements. The accuracy of the model is dictated by the number of two-port networks, a number that increases with the frequency. The equivalent circuit approach is validated with the help of an application example concerning a special type of inhomogeneous tubular structures where exact closed-form field solutions do exist.

1. INTRODUCTION

Waves and fields in inhomogeneous media is a recognized subject of major importance in electromagnetics research [1]. In a recent paper, the author proposed a matrix approach for the evaluation of the internal impedance of multilayered cylindrical structures [2]. The present work is based on [2] and elaborates on a novel, very accurate, equivalent-circuit approach for the frequency-domain representation of radially inhomogeneous cylindrical structures (solid and hollow cylinders), which allows the evaluation of the electric and magnetic fields inside the structure, as well as the evaluation of the per-unit-length internal impedance.

Boosted by the availability of increasingly powerful circuit simulators, the modeling of electromagnetic structures using equivalent-circuit approaches is a current topic of interest, in particular, when

Received 1 April 2011, Accepted 5 May 2011, Scheduled 11 May 2011
Corresponding author: Prof. J. A. Brandao Faria (brandao.faria@ieee.org).

dealing with skin effect problems [3–8]. One novelty with this work, which also deals with problems related to skin effect [9, 10], resides in the consideration of inhomogeneous materials, which can display predominant conducting properties, insulation properties, magnetic properties, or a mix of all.

Most skin-effect equivalent-circuits are concerned with homogeneous structures. They employ ladder-type circuit models which are obtained by optimizing its R and L elements considering a discrete set of sampling frequencies. A strong point with this new work is that the equivalent-circuit is derived from electromagnetic principles and its accuracy can be as higher as wished, for all frequencies under consideration.

2. BACKGROUND RESULTS

Consider a solitary inhomogeneous circular cylindrical structure of outer radius r_N. The conductivity, permeability, and permittivity of the material medium are described by radial functions $\sigma = \sigma(r)$, $\mu = \mu(r)$, and $\varepsilon = \varepsilon(r)$, for $0 < r < r_N$.

For analysis purposes the global structure is discretized into a convenient number of N homogeneous regions: $N-1$ concentric layers and 1 inner cylinder, the size of each region being chosen as deemed appropriate, taking into account the steepness or smoothness of the functions $\sigma(r)$, $\mu(r)$ and $\varepsilon(r)$. The generic nth layer is characterized by: outer radius r_n, inner radius r_{n-1}, conductivity σ_n, permeability μ_n, and permittivity ε_n (see Fig. 1 in [2]).

For time harmonic regimes, of frequency ω, each region is described by a complex wave number $\bar{k}_n$ [2],

$$\bar{k}_n = \sqrt{\omega^2 \mu_n \varepsilon_n - j\omega\mu_n\sigma_n} \tag{1}$$

The relationship between the axial electric fields and the azimuthal magnetic fields, referred to the outer an inner surfaces of the nth layer, were obtained in [2]:

$$\begin{bmatrix} \bar{E}_n \\ \bar{H}_n \end{bmatrix} = \begin{bmatrix} a_n & b_n \\ c_n & d_n \end{bmatrix} \begin{bmatrix} \bar{E}_{n-1} \\ \bar{H}_{n-1} \end{bmatrix} \tag{2}$$

where

$$a_n = \frac{\pi x'_n}{2} \left(J_1(x'_n) N_0(x_n) - J_0(x_n) N_1(x'_n) \right) \tag{3a}$$

$$b_n = \frac{\omega \pi r_n \mu_n x'_n}{2 j x_n} \left(J_0(x_n) N_0(x'_n) - J_0(x'_n) N_0(x_n) \right) \tag{3b}$$

$$c_n = \frac{j\pi x_n x'_n}{2\omega r_n \mu_n}\left(J_1(x'_n)N_1(x_n) - J_1(x_n)N_1(x'_n)\right) \tag{3c}$$

$$d_n = \frac{\pi x'_n}{2}\left(J_1(x_n)N_0(x'_n) - J_0(x'_n)N_1(x_n)\right) \tag{3d}$$

where J_ν and N_ν denote the Bessel function of the first kind and the Neumann function of order ν, respectively; and $x_n = \bar{k}_n r_n$, $x'_n = \bar{k}_n r_{n-1}$.

The homogeneous inner cylinder, of radius r_1, is characterized by a surface impedance [2], given by

$$\bar{Z}_1 = \frac{\bar{E}_1}{\bar{H}_1} = \frac{\omega\mu_1 r_1}{jx_1}\frac{J_0(x_1)}{J_1(x_1)} \quad [\Omega] \tag{4}$$

3. TWO-PORT ANALYSIS

From the view point of circuit analysis the set of layers can be interpreted as a two-port network, the output port being loaded by the impedance corresponding to the inner cylinder.

In order to define the constituent parts of the two-port network we need to make a previous change of variable. In (2), we are going to substitute the axial current intensities $\bar{I}_n$ and $\bar{I}_{n-1}$ for the azimuthal magnetic fields $\bar{H}_n$ and $\bar{H}_{n-1}$ caused by those currents

$$\bar{I}_n = \int_{S_n} (\bar{\mathbf{J}} + j\omega\bar{\mathbf{D}}) \cdot \vec{e}_z \, dS = 2\pi r_n \bar{H}_n, \quad \text{for} \quad 1 < n \leq N \tag{5}$$

where $\vec{e}_z$ is the unit vector of the axial direction and S_n is the circular surface of radius r_n. Note that the current intensity $\bar{I}'_n$ carried by the individual nth layer is obtained through

$$\bar{I}'_n = \bar{I}_n - \bar{I}_{n-1} = 2\pi\left(r_n\bar{H}_n - r_{n-1}\bar{H}_{n-1}\right) \tag{6a}$$

The global current intensity carried by the cylindrical structure is

$$\bar{I}_N = \sum_{n=1}^{N} \bar{I}'_n \tag{6b}$$

Plugging (5) into (2) we get

$$\begin{bmatrix} \bar{E}_n \\ \bar{I}_n \end{bmatrix} = \underbrace{\begin{bmatrix} a'_n & b'_n \\ c'_n & d'_n \end{bmatrix}}_{\mathbf{T}_n} \begin{bmatrix} \bar{E}_{n-1} \\ \bar{I}_{n-1} \end{bmatrix} \tag{7}$$

where

$$a'_n = a_n \ , \quad b'_n = \frac{b_n}{2\pi r_{n-1}} \ , \quad c'_n = 2\pi r_n c_n \ , \quad d'_n = d_n \frac{r_n}{r_{n-1}} \tag{8}$$

The transmission matrix $\mathbf{T}_n$ in (7), associated to the nth layer, is a unimodular matrix, whose determinant is equal to +1, (as it happens with any reciprocal multiport network [11]),

$$\det(\mathbf{T}_n) = a'_n d'_n - b'_n c'_n = (a_n d_n - b_n c_n)\,\frac{r_n}{r_{n-1}} = 1 \tag{9}$$

Note, in (9), according to [2], that $(a_n d_n - b_n c_n) = r_{n-1}/r_n$.

The set of $N-1$ layers is also globally characterized by a unimodular transmission matrix $\mathbf{T}$,

$$\begin{bmatrix} \bar{E}_N \\ \bar{I}_N \end{bmatrix} = \mathbf{T} \begin{bmatrix} \bar{E}_1 \\ \bar{I}_1 \end{bmatrix};\ \mathbf{T} = \prod_{n=2}^{N} \mathbf{T}_n = \mathbf{T}_N \cdots \mathbf{T}_n \cdots \mathbf{T}_2 = \begin{bmatrix} a & b \\ c & d \end{bmatrix} \tag{10}$$

where $\bar{E}_N$ represents the per-unit-length (pul) voltage drop measured at the outer surface of the cylindrical structure.

The inhomogeneous structure under analysis can be described indistinctly by a π-type or by a T-type equivalent circuit. We choose the T-type — see Fig. 1(a).

Due to the change of variable mentioned before, the load connected to the output port (representing the inner cylinder of radius r_1) is given, from (4), by

$$\bar{Z}_{11} = \frac{\bar{E}_1}{\bar{I}_1} = \frac{\bar{E}_1}{2\pi r_1 \bar{H}_1} = \frac{\bar{Z}_1}{2\pi r_1} = \frac{\omega\mu_1}{j2\pi x_1}\,\frac{J_0(x_1)}{J_1(x_1)} \quad [\Omega/\mathrm{m}] \tag{11}$$

The transmission matrix of the T-circuit, shown in Fig. 1(a), is readily evaluated through

$$\mathbf{T} = \begin{bmatrix} 1 + \bar{Z}_\alpha \bar{Y}_0 & \bar{Z}_\alpha + \bar{Z}_\beta + \bar{Z}_\alpha \bar{Z}_\beta \bar{Y}_0 \\ \bar{Y}_0 & 1 + \bar{Z}_\beta \bar{Y}_0 \end{bmatrix} \tag{12}$$

Comparison established between (12) and (10) leads to the determination of the series impedances $\bar{Z}_\alpha$, $\bar{Z}_\beta$ [Ω/m], and shunt admittance $\bar{Y}_0$ [Sm],

$$\bar{Z}_\alpha = (a-1)/c;\ \ \bar{Z}_\beta = (d-1)/c;\ \ \bar{Y}_0 = c \tag{13}$$

At last, the per unit length (pul) internal impedance of the cylindrical structure $\bar{Z}_{\mathrm{int}}$, which coincides with the input-port impedance of the equivalent circuit, can be evaluated from

$$\bar{Z}_{\mathrm{int}} = \frac{\bar{E}_N}{\bar{I}_N} = \bar{Z}_\alpha + \frac{1}{\bar{Y}_0 + \left(\bar{Z}_\beta + \bar{Z}_{11}\right)^{-1}} \tag{14}$$

We would like to emphasize that the equivalence between the circuit in Fig. 1(a) and the cylindrical structure itself is an equivalence that strictly speaking only applies to the input port quantities, $\bar{E}_N$ and $\bar{I}_N$. The interior of the equivalent circuit does

not have any special significance; the evaluation of the frequency-dependent parameters $\bar{Z}_\alpha$, $\bar{Z}_\beta$ and $\bar{Y}_0$ may even lead to non-realizable physical components, for example, they may exhibit negative real parts.

4. CHAIN CONNECTION OF $N-1$ TWO-PORTS

From a practical point of view, the equivalent circuit in Fig. 1(a) is of very little use, mainly because the resulting circuit elements, $\bar{Z}_\alpha$, $\bar{Z}_\beta$ and $\bar{Y}_0$, depend on the operating frequency, that is, whenever the frequency changes the equivalent circuit in Fig. 1(a) needs to be re-computed. Nonetheless, the theoretical development that led to the equivalent circuit in Fig. 1(a) is very helpful, because it can be utilized for formulating a new equivalent circuit whose intrinsic components are frequency-independent elements.

The new proposed equivalent circuit is made of the chain connection of $N-1$ two-port networks (T-type), each one corresponding to an individual layer of small thickness $t_n = r_n - r_{n-1}$.

Figure 1(b), which is identical to Fig. 1(a), depicts the two-port representation of the nth layer, where, from (13),

$$\bar{Z}_{\alpha_n} = (a'_n - 1)/c'_n; \quad \bar{Z}_{\beta_n} = (d'_n - 1)/c'_n; \quad \bar{Y}_{0_n} = c'_n \tag{15}$$

Let us start with the evaluation of $\bar{Y}_{0_n}$. Taking (15), (8), and (3c) into account we obtain

$$\bar{Y}_{0_n} = c'_n = \frac{j\pi^2 x_n x'_n}{\omega\mu_n}\left(J_1(x'_n)N_1(x_n) - J_1(x_n)N_1(x'_n)\right) \tag{16}$$

Next, the Bessel and Neumann functions $J_1(x'_n)$ and $N_1(x'_n)$ are written in the form of truncated Taylor expansions around $x_n = \bar{k}_n r_n$

$$\begin{Bmatrix} J_1(x'_n) \\ N_1(x'_n) \end{Bmatrix} \approx \begin{Bmatrix} J_1(x_n) \\ N_1(x_n) \end{Bmatrix} - \delta_n \frac{d}{dx}\begin{Bmatrix} J_1(x) \\ N_1(x) \end{Bmatrix}_{x=x_n} + \frac{1}{2}\delta_n^2 \frac{d^2}{dx^2}\begin{Bmatrix} J_1(x) \\ N_1(x) \end{Bmatrix}_{x=x_n} \tag{17}$$

where $\delta_n = (x_n - x'_n) = \bar{k}_n t_n$.

The first and second derivatives in (17) are given by, [12],

$$\begin{aligned} \frac{d}{dx}\begin{Bmatrix} J_1 \\ N_1 \end{Bmatrix} &= \begin{Bmatrix} J_0 - J_1/x \\ N_0 - N_1/x \end{Bmatrix}; \\ \frac{d^2}{dx^2}\begin{Bmatrix} J_1 \\ N_1 \end{Bmatrix} &= -\begin{Bmatrix} J_1 + J_0/x - 2J_1/x^2 \\ N_1 + N_0/x - 2N_1/x^2 \end{Bmatrix} \end{aligned} \tag{18}$$

Plugging (18) into (17), and (17) into (16), yields

$$\bar{Y}_{0_n} = \frac{j\pi^2 x_n x'_n}{\omega\mu_n}\delta_n\left(1 + \frac{\delta_n}{2x_n}\right)\left(J_1(x_n)N_0(x_n) - J_0(x_n)N_1(x_n)\right) \tag{19}$$

But, from Bessel functions theory [12], we know that

$$J_1(x_n)N_0(x_n) - J_0(x_n)N_1(x_n) = \frac{2}{\pi x_n} \tag{20}$$

Hence, we find

$$\bar{Y}_{0_n} \approx \frac{j2\pi x_n}{\omega\mu_n}\delta_n\left(1 - \frac{\delta_n}{2x_n}\right) \tag{21}$$

Taking into account that $x_n = \bar{k}_n r_n$, $\delta_n = \bar{k}_n t_n$, where $\bar{k}_n$ is given by (1), we obtain for the shunt admittance

$$\begin{cases} \bar{Y}_{0_n} \approx j2\pi r_n t_n \frac{\bar{k}_n^2}{\omega\mu_n}(1-\Delta_n) = G_{0_n} + j\omega C_{0_n} \\ G_{0_n} \approx (2\pi r_n t_n \sigma_n)(1-\Delta_n)\,; \;\; C_{0_n} \approx (2\pi r_n t_n \varepsilon_n)(1-\Delta_n) \end{cases} \tag{22}$$

where $\Delta_n = \frac{1}{2}t_n/r_n$ is a small correction factor that may be disregarded.

Therefore, we conclude that the shunt admittance is made of the parallel connection of a capacitor and a resistor. The capacitance of the capacitor is $C_{0_n} \approx 2\pi r_n t_n \varepsilon_n$ [Fm], and the conductance of the resistor is $G_{0_n} \approx 2\pi r_n t_n \sigma_n$ [Sm].

Following the same rationale the series impedances $\bar{Z}_{\alpha_n}$and $\bar{Z}_{\beta_n}$ can be determined.

After some algebra we find for $\bar{Z}_{\alpha_n}$

$$\begin{cases} \bar{Z}_{\alpha_n} = \frac{a'_n - 1}{\bar{Y}_{0_n}}; \quad a'_n = \frac{\pi x'_n}{2}\left(J_1(x'_n)N_0(x_n) - J_0(x_n)N_1(x'_n)\right) \\ a'_n - 1 \approx -\delta_n^2\frac{(1-2\Delta_n)}{2} = -\bar{k}_n^2 t_n^2\frac{(1-2\Delta_n)}{2} \\ \bar{Z}_{\alpha_n} \approx j\omega L_{\alpha_n}; \;\; L_{\alpha_n} = \frac{\mu_n}{4\pi}\frac{t_n}{r_n}(1-\Delta_n) \end{cases} \tag{23}$$

Likewise, taking into account that, [12],

$$\frac{d}{dx}\begin{Bmatrix} J_0 \\ N_0 \end{Bmatrix} = -\begin{Bmatrix} J_1 \\ N_1 \end{Bmatrix}; \quad \frac{d^2}{dx^2}\begin{Bmatrix} J_0 \\ N_0 \end{Bmatrix} = -\begin{Bmatrix} J_0 - J_1/x \\ N_0 - N_1/x \end{Bmatrix} \tag{24}$$

we find for $\bar{Z}_{\beta_n}$

$$\begin{cases} \bar{Z}_{\beta_n} = \frac{d'_n - 1}{\bar{Y}_{0_n}}; \quad d'_n = \frac{\pi x_n}{2}\left(J_1(x_n)N_0(x'_n) - J_0(x'_n)N_1(x_n)\right) \\ d'_n - 1 \approx -\frac{\delta_n^2}{2} = -\frac{\bar{k}_n^2 t_n^2}{2} \\ \bar{Z}_{\beta_n} \approx j\omega L_{\beta_n}; \;\; L_{\beta_n} = \frac{\mu_n}{4\pi}\frac{t_n}{r_n}(1+\Delta_n) \end{cases} \tag{25}$$

Therefore, from (23) and (25), we conclude that the pul series impedances $\bar{Z}_{\alpha_n}$and $\bar{Z}_{\beta_n}$are almost equal, both described by an inductor whose inductance is $L_{\alpha_n} \approx L_{\beta_n} \approx \mu_n t_n/(4\pi r_n)$ [H/m].

Figure 1(c) shows the equivalent circuit of the inhomogeneous cylindrical structure, described by the chain connection of $N-1$ two-port networks, loaded by the internal impedance $\bar{Z}_{11}$ pertaining to the inner homogeneous cylinder of radius r_1.

The radius r_1 should be chosen in a way such that $\bar{Z}_{11}$, itself, may be represented by an association of frequency-independent circuit elements. For this to be possible we have to ensure that $|x_1| = \left|\bar{k}_1 r_1\right| << 1$ for the highest frequency $\omega_{\max}$ being considered. Taking (1) into account the following condition will apply

$$r_1 << r_{1_{\max}}; \quad r_{1_{\max}} = \omega_{\max}^{-1}\mu_1^{-1/2}\left(\omega_{\max}^2\varepsilon_1^2 + \sigma_1^2\right)^{-1/4} \tag{26}$$

For $r_1 << r_{1_{\max}}$, the result in (11) leads to

$$\begin{aligned}\bar{Z}_{11} &= \frac{\omega\mu_1}{j2\pi x_1}\frac{J_0(x_1)}{J_1(x_1)} \approx \frac{\omega\mu_1}{j\pi x_1^2}\left(1-\frac{x_1^2}{8}\right) \\ &\approx \underbrace{\frac{1}{\left(\pi\sigma_1 r_1^2\right)}}_{G_1} + j\omega\underbrace{\left(\pi\varepsilon_1 r_1^2\right)}_{C_1} + j\omega\underbrace{\left(\frac{\mu_1}{8\pi}\right)}_{L_1}\end{aligned} \tag{27}$$

The equivalent circuit of the load, corresponding to the result in (27), is also shown in Fig. 1(c) — the parallel association of a resistor and a capacitor in series with and inductor; the impedance of the parallel association being much larger than the inductor's contribution.

A wealth of information can be retrieved from the equivalent circuit in Fig. 1(c).

Step 1) The pul internal impedance $\bar{Z}_{\text{int}} = \bar{Z}_{NN} = \bar{E}_N/\bar{I}_N$ can be determined using a recursive method, starting with $\bar{Z}_{11}$ and ending with $\bar{Z}_{NN}$:

$$\begin{aligned}&\bar{Z}_{11} \rightarrow \bar{Z}_{22} \rightarrow \cdots \bar{Z}_{nn} \cdots \rightarrow \bar{Z}_{N-1,N-1} \rightarrow \bar{Z}_{NN} \\ &\overbrace{\qquad\uparrow\qquad}^{\bar{Z}_{22}=\bar{Z}_{\alpha_2}+\frac{1}{\bar{Y}_{0_2}+\left(\bar{Z}_{\beta_2}+\bar{Z}_{11}\right)^{-1}}} \qquad \overbrace{\qquad\uparrow\qquad}^{\bar{Z}_{NN}=\bar{Z}_{\alpha_N}+\frac{1}{\bar{Y}_{0_N}+\left(\bar{Z}_{\beta_N}+\bar{Z}_{N-1,N-1}\right)^{-1}}}\end{aligned} \tag{28}$$

From which the pul power losses can be obtained through $P_J = \frac{1}{2}\text{Re}\left(\bar{Z}_{\text{int}}\right)\left(\bar{I}_N\bar{I}_N^*\right)$.

Step 2) Given the current intensity $\bar{I}_N$ flowing in the cylindrical structure, the pul voltage drop is obtained: $\bar{E}_N = \bar{Z}_{\text{int}}\bar{I}_N$. The output currents of the two-port networks are determined iteratively, beginning with $\bar{I}_N$ and ending with $\bar{I}_1$. Concretely, the output current of the nth T-circuit is obtained from its input-port variables using $\bar{I}_{n-1} = (1-\bar{Y}_{0_n}\bar{Z}_{\alpha_n})\bar{I}_n - \bar{Y}_{0_n}\bar{E}_n$. After gathering the current intensities $\bar{I}_N \cdots \bar{I}_n \cdots \bar{I}_1$, the radial evolution of the azimuthal magnetic field $\bar{H}(r)$ is obtained: $\bar{H}(r_n) = \bar{I}_n/(2\pi r_n)$ for $n \in [1,\ N]$.

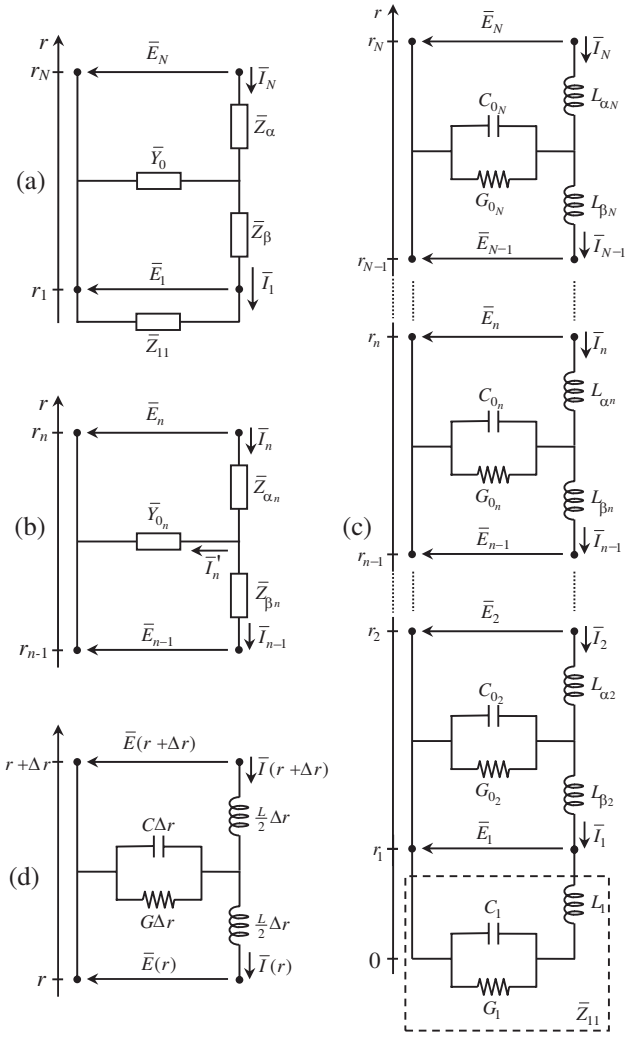

Figure 1. (a) Whole structure's equivalent circuit, where $\bar{Z}_\alpha$, $\bar{Z}_\beta$ and $\bar{Y}_0$ are complex functions of the frequency. (b) nth layer's equivalent circuit, where $\bar{Z}_{\alpha_n}$, $\bar{Z}_{\beta_n}$ and $\bar{Y}_{0_n}$ are made of frequency-independent elements. (c) Whole structure's equivalent circuit, made of the chain connection of $N-1$ two-port networks similar to the one in (b) and terminated on the load impedance $\bar{Z}_{11}$. (d) Equivalent circuit, common to all the layers, for a tubular geometry where $\sigma \propto 1/r$, $\varepsilon \propto 1/r$ and $\mu \propto r$.

Step 3) The pul output voltages of the two-port networks are determined iteratively, beginning with $\bar{E}_N$ and ending with $\bar{E}_1$. Concretely, the output pul voltage of the nth T-circuit can be obtained from $\bar{E}_{n-1} = \bar{E}_n - \bar{Z}_{\alpha_n}\bar{I}_n - \bar{Z}_{\beta_n}\bar{I}_{n-1}$. After gathering the pul voltages $\bar{E}_N \cdots \bar{E}_n \cdots \bar{E}_1$, the radial evolution of the axial electric field $\bar{E}(r)$ is obtained: $\bar{E}(r_n) = \bar{E}_n$ for $n \in [1,\ N]$.

5. EXAMPLE OF APPLICATION TO A TUBULAR STRUCTURE

The application example offered here corresponds to a rather interesting situation. Consider a solitary inhomogeneous tubular structure of inner radius r_1. The internal cylinder of radius r_1 is empty ($\sigma_1 = 0$), which means that $\bar{Z}_{11} \to \infty$ for $\omega < \omega_{\max}$ (the load of the equivalent circuit in Fig. 1(c) is practically an open circuit).

In general, the two-port networks that make up the equivalent circuit are different from layer to layer. However, from (22), (23) and (25), it can be concluded that there is a particular situation when the T-circuits turn to be equal. In fact, by enforcing the conditions

$$\forall n > 1 : \begin{cases} r_n\sigma_n = r_N\sigma_N = r\sigma(r) = \text{invariant} \\ r_n\varepsilon_n = r_N\varepsilon_N = r\varepsilon(r) = \text{invariant} \\ \mu_n/r_n = \mu_N/r_N = \mu(r)/r = \text{invariant} \\ t_n = \Delta r = (r_N - r_1)/(N-1) = \text{invariant} \end{cases} \tag{29}$$

we get

$$G_{0_n} \approx 2\pi r_N\sigma_N\Delta r,\ C_{0_n} \approx 2\pi r_N\varepsilon_N\Delta r,\ L_{\alpha_n} \approx L_{\beta_n} \approx \frac{\mu_N}{r_N}\frac{\Delta r}{4\pi} \tag{30}$$

for $1 < n \leq N$.

Therefore, each and every T-circuit is approximately characterized by the following shunt admittance and series impedance (see Fig. 1(d)):

$$\bar{Y}\Delta r \approx \underbrace{\left(2\pi r_N\left(\sigma_N + j\omega\varepsilon_N\right)\right)}_{G+j\omega C}\Delta r, \quad \bar{Z}\frac{\Delta r}{2} \approx j\omega\underbrace{\left(\frac{\mu_N}{2\pi r_N}\right)}_{L}\frac{\Delta r}{2} \tag{31}$$

5.1. Transmission Line Model

The representation in Fig. 1(d) resembles the equivalent T-circuit corresponding to a uniform transmission line of infinitesimal length Δr, without longitudinal losses but with transverse losses [13]. Such a transmission line would be described by a complex propagation

constant $\gamma = \sqrt{\bar{Z}\bar{Y}}$, and by a complex characteristic wave impedance $Z_w = \sqrt{\bar{Z}/\bar{Y}}$ [13],

$$\gamma = \sqrt{j\omega\mu_N(\sigma_N + j\omega\varepsilon_N)}; \quad Z_w = \frac{1}{2\pi r_N}\sqrt{\frac{j\omega\mu_N}{\sigma_N + j\omega\varepsilon_N}} \tag{32}$$

Hence, the chain connection of $N-1$ identical two-port networks corresponding to the tubular structure with $N-1$ layers ($N >>1$), loaded by $\bar{Z}_{11} \to \infty$, can be interpreted as a uniform transmission line of finite length $l \equiv r_N - r_1$, terminated on an open circuit load. The voltage and current evolutions along this "uniform transmission line" are given by well known results, from transmission line theory [13]:

$$\bar{E}(y) = \frac{\bar{E}_{y=0}}{1+\bar{\Gamma}}\left(e^{\gamma y} + \bar{\Gamma}e^{-\gamma y}\right); \quad \bar{I}(y) = \frac{\bar{E}_{y=0}}{Z_w(1+\bar{\Gamma})}\left(e^{\gamma y} - \bar{\Gamma}e^{-\gamma y}\right) \tag{33}$$

where $y \equiv r - r_1$, and the load reflection coefficient is $\bar{\Gamma} = 1$ for an open line. Therefore, (33) transforms into

$$\bar{E}_n = \bar{E}_1 \cosh\left(\gamma(r_n - r_1)\right); \quad \bar{I}_n = \frac{\bar{E}_1}{Z_w}\sinh\left(\gamma(r_n - r_1)\right) \tag{34}$$

for $n \in [1,\ N]$.

The input impedance of the transmission line, which is to be identified with the pul internal impedance of the tubular conductor, is given by $\bar{Z}_{input} = \bar{E}_N/\bar{I}_N = \bar{Z}_{\text{int}} = Z_w \coth(\gamma l)$; taking (34) into account we may write

$$\bar{Z}_{\text{int}} = \underbrace{\left(\frac{1}{2\pi r_N}\sqrt{\frac{j\omega\mu_N}{\sigma_N + j\omega\varepsilon_N}}\right)}_{Z_w} \coth(\underbrace{\sqrt{j\omega\mu_N(\sigma_N + j\omega\varepsilon_N)}}_{\gamma}(r_N - r_1)) \tag{35}$$

The rationale for the results in (34)–(35) was based on the properties of the equivalent circuit developed in Sections 3 and 4. Based on direct integration of Maxwell equations, employing the magnetic vector potential as primary field, a purely theoretical validation of (34)–(35) is offered in Appendix A. With that validation, sound evidence is provided concerning the consistency of the equivalent circuit in Fig. 1(c).

5.2. Numerical Results and Discussion

For illustration purposes consider a solitary inhomogeneous tubular conductor characterized by the following data: $r_N = 4\,\text{mm}$, $r_1 = 2\,\text{mm}$, $\sigma_N = 5 \times 10^6\,\text{S/m}$, $\mu_N = 2\mu_0$, and satisfying (29).

In a good conductor the displacement current can be neglected up into the optical frequency range, [13], therefore, the term $\omega\varepsilon_N$ will be disregarded. Consequently, the results in (31) lead to: $\bar{Y} = G \approx 2\pi r_N \sigma_N = 125.7\,\text{kS}$; $\bar{Z} = j\omega L$; $L \approx \mu_N/(2\pi r_N) = 0.1\,\text{mH}$.

A useful parameter for the analysis of skin effect phenomena in conducting materials is the skin depth $\delta_{skin} = (\pi f \mu_N \sigma_N)^{-1/2}$, which, in this example, is a radially invariant parameter. Taking into account the values assigned to μ_N and σ_N we get

$$\delta_{skin} = \frac{\xi}{\sqrt{f}};\ \ \xi = 0.159\ \text{ms}^{-1/2} \tag{36}$$

Next, the pul internal impedance of the tubular conductor was computed using (28), from the equivalent circuit approach, which leads to a finite continued fraction [14], with N terms

$$\bar{Z}_{\text{int}}(\omega) = j\omega L\frac{\Delta r}{2} + \cfrac{1}{G\Delta r + \cfrac{1}{j\omega L\Delta r + \cfrac{1}{G\Delta r + \cfrac{1}{\vdots \;\; j\omega L\Delta r + \cfrac{1}{G\Delta r}}}}}} \tag{37}$$

The accuracy of (37) depends on the number N of terms involved in the continued fraction, that is, depends on the number of chained T-circuits that make up the equivalent circuit in Fig. 1(c). In fact, the validity of the truncated Taylor expansions utilized in Section 4 (see eqn (19)) requires that $|\delta_n| = \left|\bar{k}\Delta r\right| << 1$ or, in other words

$$N >> (r_N - r_1)/\delta_{skin} \ \rightarrow \ \ N >> 12.57 \times 10^{-3}\sqrt{f\ [\text{Hz}]} \tag{38}$$

The higher the frequency the larger the number of two-port networks necessary.

For example, for $f = 0.1\,\text{MHz}$, we must have $N>>4$. We chose $N = 40$.

Figure 2 shows computation results for the pul internal impedance, $\bar{Z}_{\text{int}} = R(\omega) + jX(\omega)$, for a frequency sweeping from 0 to 0.1 MHz. Circle marks correspond to the equivalent circuit approach (Eqn. (37)), whereas the solid lines correspond to the exact theoretical result in (A14). The agreement is remarkable.

Setting $\bar{I}_N = 1\,\text{A}$, and following the procedure outlined at the end of Section 4 (steps 2 and 3) we have also computed the voltages and currents at the successive ports of the equivalent circuit. Next, that information being accounted, we plotted the radial variation of the absolute values of the electric and magnetic field strengths, E_n, H_n,

for $n \in [1, N]$, with $N = 40$. The corresponding results, identified by circle marks, are shown in Fig. 3 and Fig. 4, where, in addition, and for comparison purposes, the exact theoretical results from (A10) and (A11) are also represented (solid lines). The graphical plots depicted in Fig. 3 and Fig. 4 were obtained for $f = 0.1\,\text{kHz}$ and $f = 0.1\,\text{MHz}$. Again, the agreement between exact and approximate results is remarkable.

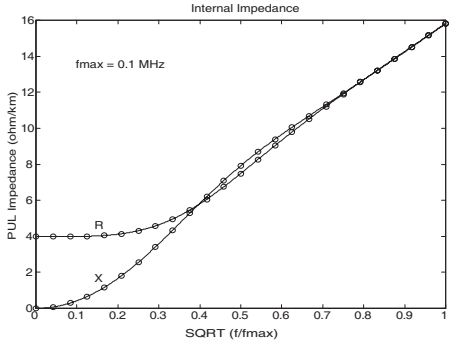

Figure 2. Real and imaginary parts of the per-unit-length internal impedance against frequency in the range 0 to 0.1 MHz. Solid lines are theoretical curves from (A14). Circle marks were obtained using the equivalent circuit approach, with $N = 40$.

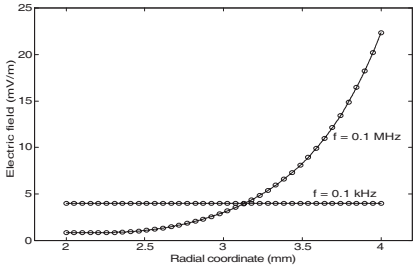

Figure 3. Radial evolution of the magnitude of the electric field for $I_N = 1\,\text{A}$, $f = 0.1\,\text{kHz}$, and $f = 0.1\,\text{MHz}$. Solid lines are theoretical curves from (A10). Circle marks were obtained using the equivalent circuit approach, with $N = 40$.

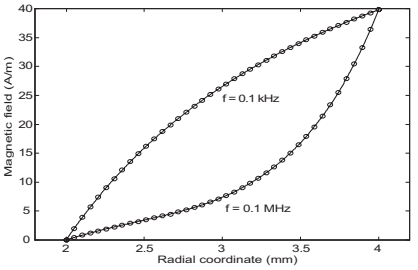

Figure 4. Radial evolution of the magnitude of the magnetic field for $I_N = 1\,\text{A}$, $f = 0.1\,\text{kHz}$, and $f = 0.1\,\text{MHz}$. Solid lines are theoretical curves from (A11). Circle marks were obtained using the equivalent circuit approach, with $N = 40$.

6. CONCLUSION

Inhomogeneous structures find application in many areas from microwaves to power systems. In this work attention was paid to radially inhomogeneous cylindrical structures, where the constitutive medium can be a conductor, a dielectric, a magnetic material, or a mix of all them.

An equivalent circuit consisting in a cascade of N two-port networks (T-type), with frequency-independent R, L and C elements, was proposed to accurately simulate the behavior of inhomogeneous structures. The accuracy of the developed model is as higher as wished, since it only depends on the number of T-circuits being employed — such a number typically increases with the square-root of the frequency. The presented approach permits not only the computation of the per-unit-length internal impedance of the solitary cylindrical structure, but also the evaluation of the radial variations of the electric and magnetic fields inside the structure. The equivalent-circuit model was validated by resorting to an application example of an inhomogeneous tubular conductor, characterized by $\mu \propto r$ and $\sigma \propto 1/r$, for which simple, but exact, closed-form solutions are available.

Inhomogeneous solitary cylindrical structures were dealt with here and in [2]. However, ordinary real structures do include more than one cylinder, like, for example, multilayered conductors belonging to multiconductor cables. In the latter case skin and proximity effects are interlinked. Their analysis, in the framework of inhomogeneous structures, is suggested for future work.

APPENDIX A.

Radially inhomogeneous cylindrical structures have been analyzed in a recently published paper [2], where from

$$\begin{cases} \nabla \times \bar{\mathbf{H}} = (\sigma + j\omega\varepsilon)\bar{\mathbf{E}} \\ \nabla \times \bar{\mathbf{E}} = -j\omega\mu\bar{\mathbf{H}} \end{cases} \quad \rightarrow \quad \begin{cases} \nabla^2\bar{\mathbf{A}} + \bar{k}^2\bar{\mathbf{A}} = 0 \\ \bar{\mathbf{E}} = -j\omega\bar{\mathbf{A}} \\ \bar{\mathbf{H}} = \nabla \times \bar{\mathbf{A}}/\mu \end{cases}$$

an equation for the complex amplitude of the axial magnetic vector potential $\mathbf{A}$ was obtained

$$r^2\frac{d^2\bar{A}}{dr^2} + \left(1 - \frac{r}{\mu(r)}\frac{d\mu(r)}{dr}\right) r\frac{d\bar{A}}{dr} + \left(r\,\bar{k}(r)\right)^2\bar{A} = 0 \qquad \text{(A1)}$$

where $\bar{k}^2(r) = -j\omega\mu(r)\,(\sigma(r) + j\omega\varepsilon(r))$, for $r_1 < r < r_N$.

The evaluation of $\bar{A}(r)$ on the cylinder's outer radius, $r = r_N$, permits the determination of the pul internal impedance of the

structure

$$\bar{Z}_{\text{int}} = \frac{\bar{E}_N}{\bar{I}_N} = \frac{-j\omega\bar{A}(r_N)}{\bar{I}_N} \tag{A2}$$

where $\bar{I}_N$ is the structure's total current intensity, and $\bar{E}_N = \bar{E}(r_N)$.

Considering that the radial variations of $\varepsilon(r)$, $\sigma(r)$, and $\mu(r)$ are such that (A1) can be transformed into an Euler-Cauchy equation [15], a general closed-form analytical solution for the magnetic vector potential in the form of a sum of two complex powers of r was obtained in [15]. Here, however, we offer a new, simpler, particular solution for (A1), which can be expressed in terms of two exponential functions.

Let

$$1 - \frac{r}{\mu(r)}\frac{d\mu(r)}{dr} = 0 \quad \rightarrow \quad \mu(r) = \mu_N \left(\frac{r}{r_N}\right) \tag{A3}$$

Next, consider that $\bar{k}$ is radially invariant, which requires

$$\left\{ \begin{array}{c} \sigma(r) \\ \varepsilon(r) \end{array} \right\} = \frac{r_N}{r} \left\{ \begin{array}{c} \sigma_N \\ \varepsilon_N \end{array} \right\} \quad \rightarrow \quad \bar{k}^2 = -j\omega\mu_N \left(\sigma_N + j\omega\varepsilon_N\right) \tag{A4}$$

Plugging (A3) and (A4) into (A1) leads to the trivial equation

$$\frac{d^2\bar{A}}{dr^2} + \bar{k}^2\bar{A} = 0 \tag{A5}$$

whose solution is

$$\bar{A}(r) = A_1\, e^{\gamma r} \; + A_2\, e^{-\gamma r} \tag{A6}$$

where γ, the so-called complex propagation constant, is given by

$$\gamma = j\bar{k} = \sqrt{j\omega\mu(r)\left(\sigma(r) + j\omega\varepsilon(r)\right)} = \sqrt{j\omega\mu_N\left(\sigma_N + j\omega\varepsilon_N\right)} \tag{A7}$$

The azimuthal magnetic field, associated to $\mathbf{A}$, is obtained from

$$\bar{H}(r) \; = -\frac{1}{\mu(r)}\frac{d}{dr}\bar{A}(r) = \frac{-\gamma}{\mu(r)}\left(A_1\, e^{\gamma r} - A_2\, e^{-\gamma r}\right) \tag{A8}$$

By enforcing the boundary conditions at the inner ($r = r_1$) and outer ($r = r_N$) radius of the solitary tubular cylindrical structure, i.e., $\bar{H}(r_1) = 0$ and $\bar{H}(r_N) = \bar{I}_N/(2\pi r_N)$, a solution for the complex constants A_1 and A_2 is found

$$\left\{ \begin{array}{c} A_1 \\ A_2 \end{array} \right\} = \frac{-\mu_N\bar{I}_N}{4\pi r_N\gamma} \times \frac{1}{\sinh\left(\gamma(r_N - r_1)\right)} \times \left\{ \begin{array}{c} e^{-\gamma r_1} \\ e^{+\gamma r_1} \end{array} \right\} \tag{A9}$$

Plugging (A9) into (A6), and into (A8), gives the electric and magnetic field radial variations inside the inhomogeneous tubular structure

$$\bar{E}(r) \; = \; -j\omega\bar{A}(r) = \frac{j\omega\mu_N\bar{I}_N}{2\pi r_N\gamma} \times \frac{\cosh\left(\gamma(r - r_1)\right)}{\sinh\left(\gamma(r_N - r_1)\right)} \tag{A10}$$

$$\bar{H}(r) \; = \; \frac{\bar{I}_N}{2\pi r} \times \frac{\sinh\left(\gamma(r - r_1)\right)}{\sinh\left(\gamma(r_N - r_1)\right)} \tag{A11}$$

The pul internal impedance of the structure, (A2), is determined by making $r = r_N$ in (A10), yielding

$$\bar{Z}_{\text{int}} = \frac{j\omega\mu_N}{2\pi r_N \gamma} \coth\left(\gamma(r_N - r_1)\right) = \frac{1}{2\pi r_N}\sqrt{\frac{j\omega\mu_N}{\sigma_N + j\omega\varepsilon_N}} \coth\left(\gamma(r_N - r_1)\right) \tag{A12}$$

If the cylindrical structure is made of a good conducting medium, where $\omega\varepsilon << \sigma$, then (A7) and (A12) can be simplified

$$\gamma = \sqrt{j\omega\mu_N\sigma_N} = \frac{1+j}{\delta_{skin}} \tag{A13}$$

$$\bar{Z}_{\text{int}} = \frac{1+j}{2\pi r_N \sigma_N \delta_{skin}} \coth\left((1+j) \times \frac{r_N - r_1}{\delta_{skin}}\right) \tag{A14}$$

where δ_{skin} is the skin effect penetration depth, $\delta_{skin} = \sqrt{2/(\omega\mu_N\sigma_N)}$ [13].

REFERENCES

1. Chew, W. C., *Waves and Fields in Inhomogeneous Media*, IEEE Press, New York, USA, 1995.
2. Faria, J. A., "A matrix approach for the evaluation of the internal impedance of multilayered cylindrical structures," *Progress In Electromagnetics Research B*, Vol. 28, 351–367, 2011.
3. Dinh, T. V., B. Cabon, and J. Chilo, "New skin-effect equivalent circuit," *Elect. Letters*, Vol. 26, No. 19, 1582–1584, 1990.
4. Kim, S. and D. Neikirk, "Compact equivalent circuit model for the skin effect," *IEEE MTT-S Int. Microwave Symp. Digest*, Vol. 3, 1815–1818, San Francisco, USA, 1996.
5. Sen, B. K. and R. Wheeler, "Skin effects models for transmission line structures using generic SPICE circuit simulators," *IEEE 7th Topical Meeting on Elect. Performance of Elect. Packaging*, 128–131, West Point, USA, 1998.
6. Mei, S. and Y. Ismail, "Modeling skin effect with reduced decoupled R-L circuits," *Proc. Int. Symp. on Circuits and Systems*, Vol. 4, 588–591, Bangkok, Thailand, 2003.
7. Mei, S. and Y. Ismail, "Modeling skin and proximity effects with reduced realizable RL circuits," *IEEE Trans. VLSI Systems*, Vol. 12, No. 4, 437–447, 2004.
8. Wang, C., H. Liao, C. Li, R. Huang, W. Wong, X. Zhang, and Y. Wang, "A wideband predictive double-π equivalent-circuit for on-chip spiral inductors," *IEEE Trans. Electron Devices*, Vol. 56, No. 4, 609–619, 2009.

9. Silveira, F. and J. Lima, "Skin effect from extended irreversible thermodynamics perspective," *Journal of Electromagnetic Waves and Applications*, Vol. 24, No. 2/3, 151–160, 2010.
10. Lovric, D., V. Boras, and Vujevic, "Accuracy of approximate formulas for internal impedance of tubular cylindrical conductors for large parameters," *Progress In Electromagnetics Research M*, Vol. 16, 171–185, 2011.
11. Faria, J. A., "On the transmission matrix of 2n-port reciprocal networks," *Microwave and Opt. Tech. Letters*, Vol. 33, No. 3, 151–154, 2002.
12. Watson, G., *A Treatise on the Theory of Bessel Functions*, Cambridge University Press, 1922.
13. Faria, J. A., *Electromagnetic Foundations of Electrical Engineering*, Wiley, Chichester, UK, 2008.
14. Khinchin, A. Y., *Continued Fractions*, Dover, New York, USA, 1997.
15. Brandao Faria, J. A., "Skin effect in inhomogeneous Euler-Cauchy tubular conductors," *Progress In Electromagnetics Research M*, Vol. 18, 89–101, 2011.